Proceedings of Global Power and Propulsion Society
ISSN-Nr: 2504-4400
GPPS Chania22
18th–20th September, 2022

www.gpps.global

GPPS-TC-2022-0077

INFLUENCE OF AXIAL AIR INJECTION ON THE FLAME STABILITY OF A TECHNICALLY PREMIXED HYDROGEN FLAME

Daniel Mira
Barcelona Supercomputing Center (BSC)
daniel.mira@bsc.es
Barcelona, Spain

Ambrus Both
Barcelona Supercomputing Center (BSC)
ambrus.both@bsc.es
Barcelona, Spain

Anurag Surapaneni
Barcelona Supercomputing Center (BSC)
anurag.surapaneni@bsc.es
Barcelona, Spain

ABSTRACT

This work is a numerical investigation on the stability of a hydrogen flame in a swirl-stabilized burner configuration using large-eddy simulation with tabulated chemistry. Experimental results from this combustor showed that the axial injection influences the vortex breakdown (VB) position and therefore, the propensity of the burner to produce flashback. It is found that depending on the combination of primary swirl flow and amount of axial air injection, the flow can exhibit self-excited oscillations, and more importantly, it can control the flashback safety. Numerical simulations are used here to investigate different combinations of axial air injection and evaluate its impact on flame stability and flashback resistance. It is found that the axial air injection influences the flame stabilization and the position of the central recirculation zone. The penetration of the flame in the mixing tube introduces a strong expansion and acceleration of the flow, which results in a reduction of the spreading angle and eventually a flashback event.

INTRODUCTION

Current emissions regulations and decarbonization targets in the energy and aviation sectors are pushing the use of hydrogen-enriched fuels for gas turbine applications (Tang et al., 2014). Hydrogen emerges as an interesting alternative for combustion systems with the potential to contribute significantly to the decarbonization of a variety of energy applications (Khandelwal et al., 2013; Onarheim et al., 2020; Lee et al., 2010). This potential comes with the demand on future burner designs to accommodate a multitude of fuels with varying, but high, amounts of hydrogen (Mayer et al., 2012), while allowing for a wide stability range, high efficiency and low NO_x emissions. From these requirements, the investigation of burner designs to operate on pure hydrogen can establish a benchmark for many upcoming high-reactivity fuel combustors, leading to insights that can have a significant effect on a wide variety of future energy applications Cheng et al. (2009); Chterev and Boxx (2021).

Flame stabilization is one of the major factors to be considered for the safe operation of hydrogen in gas turbine burners Palies (2020). A burner design to operate with hydrogen-air mixtures building upon the concept of central non-swirling axial air injection (AI) for flashback (FB) prevention was developed by Reichel, Terhaar and Paschereit (2015) (Reichel, Goeckeler and Paschereit, 2015; Reichel and Paschereit, 2017; Reichel et al., 2018). This burner concept was introduced by Burmberger and Sattelmayer (2011) to increase the operational range of swirl burners. The axial air injection is used to correct the velocity deficit caused by the swirling flow and provide a mechanism for flashback resistance. While hydrocarbon flames can be stabilized in flow fields with high swirl numbers and a strong bubble shaped vortex breakdown close to the burner exit, hydrogen flames require less swirled air and stronger axial air injection to ensure flame stability and safe operation. This strategy causes a delay in the vortex breakdown, but prevents the flashback formation (Sangl et al., 2011).

Reichel et al. (2018) showed experimentally, that without AI, the central recirculation zone (CRZ) caused by the vortex break down (VB), which is necessary for flame anchoring, extends close or even into mixing tube for some operating

conditions, showcasing a deficit in axial velocity on the central axis of the mixing tube. This is typical for high swirl, low-reacting fuel combustors (Tanneberger et al., 2015; Mira et al., 2018), but can lead to FB if high reacting fuels are used (Mayer et al., 2012). Using different rates of AI, which can be quantified by the ratio of axially injected, non-swirling air flow to total air flow $\chi = \dot{V}_{\mathrm{ax}}/(\dot{V}_{\mathrm{ax}} + \dot{V}_{\mathrm{swirl}})$, it could be shown for a medium AI rate ($\chi = 7.5\%$) that it overcomes the axial velocity deficit partially over the length of the mixing tube, while not displacing the VB further downstream. In contrast, a high rate of AI ($\chi = 12.5\%$) could overcome the axial velocity deficit over the whole mixing tube pushing the VB downstream into the combustion chamber. This strategy allows an increase in FB resistance, as the flow profile at the mixing tube outlet approaches the ideal plug-like flow shape (Reichel, Terhaar and Paschereit, 2015), which was also demonstrated by numerical simulations in the work by Mira et al. (2020). Reichel, Terhaar and Paschereit (2015) have shown that the AI reduces the initial swirl number. Note that high swirl ensures a compact flame attached to the burner exit, but lower swirl is favourable for FB resistance due to simpler axial velocity deficit compensation.

In the present study, the focus is given to evaluate the influence of the axial air injection on the flame stability of a hydrogen burner starting from a stable operating point that has been well characterized experimentally. Different cases featuring lower levels of axial air injection are defined in order to evaluate the flow fields and flame dynamics as the axial air injection is reduced to the flashback point. This work is an extension of our previous work (Mira et al., 2020) where the hydrogen-air mixing is accounted for and the impact of fluctuations in equivalence ratio and fuel heterogeneity are also included. This modelling approach is extended to evaluate the impact of axial air injection on flame stabilization for a constant global equivalence ratio, which was more difficult to conduct in experiments due to the distribution of flow rates across the different components by pressure loss.

METHODOLOGY

Governing equations

The equations describing the flow field correspond to the low-Mach number approximation of the Navier-Stokes equations with the energy equation represented by the total enthalpy. The Favre-filtered governing equations for LES correspond to the continuity, momentum and enthalpy and read as:

$$\frac{\partial \bar{\rho}}{\partial t} + \nabla \cdot (\bar{\rho}\widetilde{\mathbf{u}}) = 0, \tag{1}$$

$$\partial_t (\overline{\rho}\widetilde{\mathbf{u}}) + \nabla \cdot (\overline{\rho}\widetilde{\mathbf{u}}\widetilde{\mathbf{u}}) = -\nabla \cdot \overline{\tau}_M - \nabla \overline{p} + \nabla \cdot \tau(\widetilde{\mathbf{u}}), \tag{2}$$

$$\frac{\partial \overline{\rho}\widetilde{h}}{\partial t} + \nabla \cdot \left(\overline{\rho}\widetilde{\mathbf{u}}\widetilde{h}\right) = -\nabla \cdot \overline{\tau}_h + \nabla \cdot \left(\bar{\rho}\widetilde{D}\nabla\widetilde{h}\right). \tag{3}$$

where standard notation is used for all the quantities with $\bar{\rho}$, $\widetilde{\mathbf{u}}$, $\widetilde{h}$, $\widetilde{D}$, $\bar{p}$ and $\bar{\mu}$ represent the density, velocity vector, total enthalpy (sensible and chemical), diffusivity, pressure and dynamic viscosity using filtered quantities. The τ term stands for the unresolved or subgrid terms related to the filtering operation and applies to the unresolved momentum flux $\overline{\tau}_M$ and the unresolved enthalpy flux $\overline{\tau}_h$. The subgrid viscous stress tensor is determined based on the Stoke's assumption and the turbulence contribution is obtained by the use of the Boussinesq approximation (Poinsot and Veynante, 2005). A unity Lewis number assumption has been made to simplify the scalar transport in the governing equations. Heating due to viscous forces is neglected in the enthalpy equation and the unresolved heat flux is modelled using a gradient diffusion approach (Mira et al., 2014). The modelling framework is closed by an appropriate expression for the subgrid-scale viscosity. The eddy-viscosity is obtained from the Vreman (2004) model using a constant $c_k = 0.1$. The same single-value constant has been used in previous studies and it is also retained here (Both et al., 2020; Mira et al., 2020).

The flame structure of this non-premixed flame is determined by the flamelet method (Mira et al., 2020). Based on the characteristics of the mixing field, a tabulation of premixed laminar flames is used for the construction of the thermo-chemical database. The flamelet database uses the chemistry from the full San Diego mechanism (Che, 2016), which demonstrated excellent performance for predicting hydrogen flames in a variety of flow conditions (Zheng et al., 2013; Mira et al., 2014, 2020) and is also retained here. Burner stabilized premixed flamelets are used to account for the enthalpy variation due to heat loss (Gövert et al., 2018). Three controlling variables are used to characterize the thermochemical state of the laminar flame structure composing the manifold: mixture fraction Z, progress variable Y_c, and normalized enthalpy i. In order to account for turbulent/chemistry interactions at the subgrid scale, the tabulated properties from the manifold are integrated with a presumed-shape probability density function (PDF). This PDF describes the statistical effect of turbulence on the flame structure (Domingo et al., 2008), leading to a five-dimensional flamelet database extended by the variances of mixture fraction $Z_v = \widetilde{Z^2} - \widetilde{Z}\widetilde{Z}$ and progress variable $Y_{c,v} = \widetilde{Y_c^2} - \widetilde{Y}_c\widetilde{Y}_c$ respectively. The systems of equations read:

$$\frac{\partial \overline{\rho}\widetilde{Z}}{\partial t} + \nabla \cdot \left(\overline{\rho}\widetilde{\mathbf{u}}\widetilde{Z}\right) = -\nabla \cdot \overline{\tau}_Z + \nabla \cdot \left(\bar{\rho}\bar{D}\nabla\widetilde{Z}\right), \tag{4}$$

$$\frac{\partial \overline{\rho}\widetilde{Y}_c}{\partial t} + \nabla \cdot \left(\overline{\rho}\widetilde{\mathbf{u}}\widetilde{Y}_c\right) = -\nabla \cdot \overline{\tau}_{Y_c} + \nabla \cdot \left(\bar{\rho}\bar{D}\nabla\widetilde{Y}_c\right) + \overline{\dot{\omega}}_{Y_c}, \tag{5}$$

$$\frac{\partial \overline{\rho}Z_v}{\partial t} + \nabla \cdot (\overline{\rho}\widetilde{\mathbf{u}}Z_v) = -\nabla \cdot \overline{\tau}_{Z_v} + \nabla \cdot (\bar{\rho}\bar{D}\nabla Z_v) - 2\overline{\tau}_Z \cdot \nabla\widetilde{Z} - 2\overline{s}_{\chi_Z}, \tag{6}$$

$$\frac{\partial \overline{\rho}Y_{c,v}}{\partial t} + \nabla \cdot (\overline{\rho}\widetilde{\mathbf{u}}Y_{c,v}) = -\nabla \cdot \overline{\tau}_{Y_{c,v}} + \nabla \cdot (\bar{\rho}\bar{D}\nabla Y_{c,v}) - 2\overline{\rho}\overline{s}_{\chi_{Y_c}} + 2\overline{Y_c\dot{\omega}}_{Y_c}. \tag{7}$$

The unresolved terms $\overline{\tau}_Z$ and $\overline{\tau}_{Y_c}$ are closed using a gradient diffusion approach Domingo et al. (2008). The term $\overline{\dot{\omega}}_{Y_c}$ is the filtered progress variable source term, while $\overline{s}_{\chi_Z}$ and $\overline{s}_{\chi_{Y_c}}$ are the unresolved part of the scalar dissipation rate for mixture fraction and progress variable respectively, which are modeled assuming a linear relaxation of the variance within the subgrid (Domingo et al., 2008) and are given by:

$$\overline{s}_{\chi_Z} = \overline{\rho}\frac{Z_v}{\Delta^2/\nu_t}, \tag{8}$$

$$\overline{s}_{\chi_{Y_c}} = \overline{\rho}\frac{Y_{c,v}}{\Delta^2/\nu_t}, \tag{9}$$

where Δ is the filter length obtained from the mesh and ν_t is the eddy viscosity.

Numerical methods

These modelling framework has been developed in the multiphysics code Alya (Vázquez et al., 2016). The discretization strategy is based on low-dissipation low-Mach number solver using linear finite elements (Both et al., 2020).The stabilisation is only introduced for the continuity equation by means of a non-incremental fractional-step method, modified in order to account for variable density flows. The final scheme preserves momentum and angular momentum for variable density flows. The error of kinetic energy conservation is of order $O(dt \cdot h^{(k+1)})$, thus dissipation is limited. Standard stabilised finite elements are used for the scalars, while the time integration is carried out by means of an explicit third order Runge-Kutta scheme for momentum and scalars.

Computational cases

The operational conditions simulated in this case are derived from the stable operation point of the burner for a lean equivalence ratio at $\phi = 0.6$ (Reichel et al., 2018) used as baseline. The Reynolds number at which the burner operates is Re = 75000 based on the mixing tube diameter. Air is pre-heated at $T_{air} = 453$K and hydrogen at $T_{H2} = 320$K. Burner geometry can be found in the experimental papers (Reichel et al., 2018; Reichel and Paschereit, 2017) and previous numerical work (Mira et al., 2018, 2020). From this baseline condition, three computational cases were derived featuring different levels of axial air injection AI respect to the reference case AI_0, and those are Case 1-0.9AI_0, Case 2-0.8AI_0 and Case 3-0.75AI_0. Note that all cases feature the same air and fuel flow rates, so the global equivalence ratio is the same, but the ratio between the central injection and swirling air differs.

RESULTS AND DISCUSSION

This section is divided into three main parts dedicated to the validation of the mean flow field with the PIV data from (Reichel et al., 2018), the analysis of stable cases using different ratios of axial air injection and a final section showing the flashback case. As the case with the lowest axial air injection Case 3-0.75AI_0 leads to flashback, this case is included in the last section.

Validation of the stable operating point

A comparison of the flow field for the stable operation point with $\phi = 0.6$ between LES and PIV is shown in Fig. 1. Radial profiles of the mean axial velocity and fluctuations at different axial locations are shown for comparison. The profiles show a good correlation between the LES and PIV for the mean quantities, but only for the fluctuations in the most upstream locations. This can be explained by the lower resolution considered downstream the flame front that is not sufficient to correctly describe the second order statistics. Nevertheless, the good correlation in mean quantities confirms the proposed modelling approach is valid to recover the correct flame propagation in this case and ensures a correct flame stabilization mechanism. The size and location of the central and corner recirculations are well predicted and the spreading rates are also in good agreement with the PIV measurements. The plots show, that the LES matches well the velocity deficit

at the upstream location where the flame is stabilized and the correlation with the PIV also extends to the formation of the central recirculation and the spreading angle.

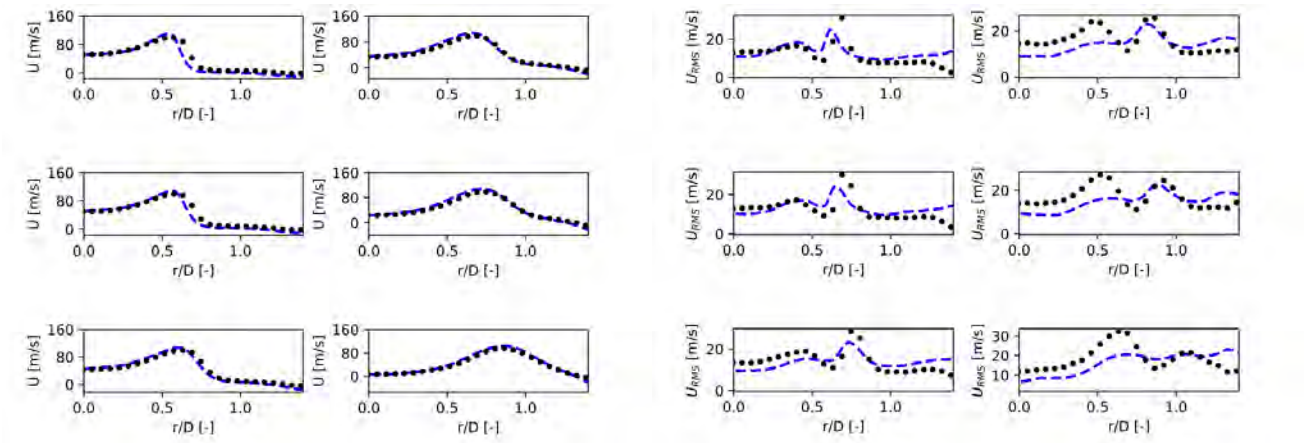

(a) Mean Axial velocity

(b) Axial velocity fluctuations

Figure 1 Comparison of the reacting numerical simulations with the experimental PIV data (Reichel and Paschereit, 2017) for Case 1-0.9Al$_0$ at different axial locations: mean axial velocity (a) and fluctuations (b). Dashed line: LES present work, symbols: experimental data

Stable operating points with lower axial air injection

The results from the stable operating points Baseline, Case 1 and Case 2 are presented in this section. Contour plots of mean axial velocity and mean temperature are shown in Figs. 2 and 3 respectively. The distribution of axial velocity across the middle plane of the combustor clearly illustrates the effects on axial air injection on the flow field. The velocity field shows a region with low velocity at the position of the flame tip caused by the flow dilation due to the heat release, which can be distinguished for all the three cases. As the axial air injection is reduced, the flame tends to stabilize at more upstream locations and this low velocity region is displaced upstream. The central recirculation zone is also displaced upstream confirming the experimental observations.

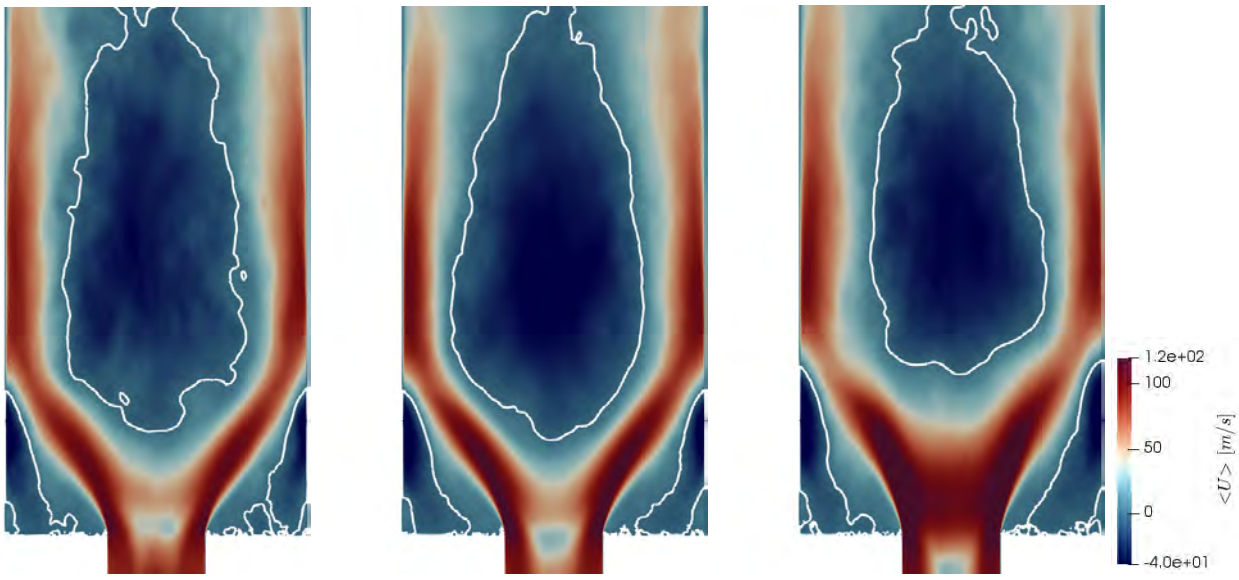

Figure 2 Mean axial velocity field at the middle plane of the combustion chamber with iso-contour of $U = 0$ [m/s] for Baseline (left), Case 1 (middle) and Case 2 (right).

While Case I shows a similar velocity field to the baseline case, Case II reveals a strong acceleration of the flow at the entrance of the combustion chamber that extends downstream. This strong acceleration occurs because the flame has stabilized partially in the mixing tube, as can be clearly seen in Fig. 3. The penetration of the flame in the mixing tube introduces a strong expansion and acceleration of the flow, which results in a reduction of the spreading angle. As the flame tip is located inside the mixing tube, the flame is shifted to richer mixtures and higher temperatures are found in this

case. The extreme case occurs when the axial momentum is not able to sustain the flame propagation and the flashback is produced, as seen for Case 3 in Fig. 6.

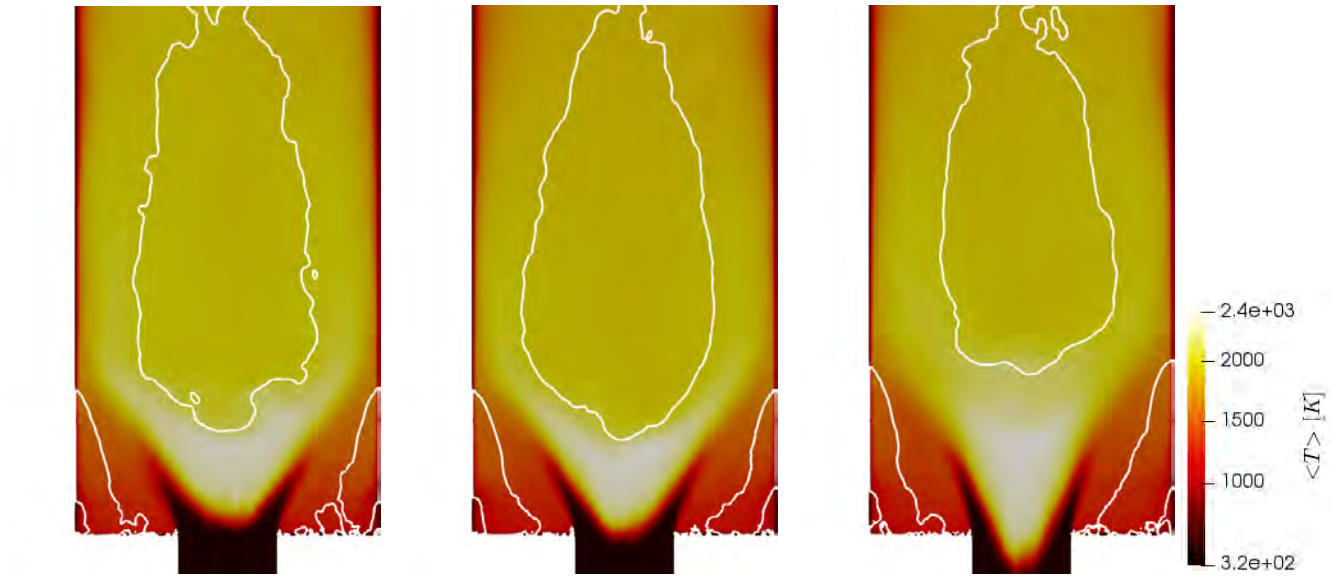

Figure 3 Mean temperature field at the middle plane of the combustion chamber with iso-contour of $U = 0$ [m/s] for Baseline (left), Case 1 (middle) and Case 2 (right).

To further evaluate the combustion characteristics of the stable operating points, scatter plots of the time-averaged mixture fraction Z and temperature T fields are plotted in three distinctive regions of the burner. These regions include the flame tip, and the inner and outer layers of flame, see Fig. 4. In the flame tip region, the most reactive mixture fraction becomes richer as the axial momentum is reduced evidencing the upstream movement of the flame. The inner reacting zone widens with lower axial momentum as the flame faces a richer mixture and burns faster. Finally, changes in the the outer region are not as severe, this is the result of the negligible changes in the flame shape in this region. The scatter plots show the upstream movement of the flame results in rich burning and higher flame propagation, which also contributes to the flashback phenomena.

In order to better understand how the flame adapts to the changes in axial air injection, profiles of mean velocity at different axial locations are shown for comparison in Fig. 5. The plots show the evolution of the velocity profiles as they develop along the mixing tube from the plane where the axial air injection intersects with the swirling flow (from top-left to bottom-right). The profiles indicate that the higher level of axial air injection corrects the velocity deficit on the centerline that is generated by the swirled flow, see Case 2 compared to the Baseline and Case 1. The differences in magnitude are quite large and are retained across the mixing tube until the flow approaches the combustion chamber, see the first and second row of the right column. In this region, as the flame has stabilized near the nozzle exit (Case 1) and partially inside the mixing tube (Case 2), an acceleration of the flow is observed. This can be clearly seen in the bottom right plot, where

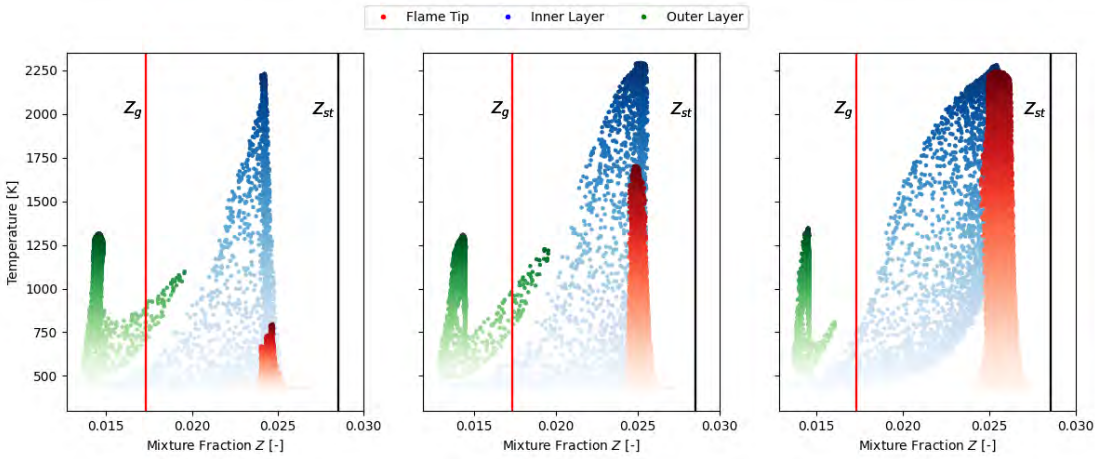

Figure 4 Mixture fraction Z and temperature T scatter plots for for Baseline (left), Case 1 (middle) and Case 2 (right).

Case 2 shows a higher axial velocity than the Baseline case. This acceleration is caused by the flow dilation and is a direct consequence of the anchoring of the flame. From the distribution of axial velocity, it can be observed that the Baseline case shows an almost uniform velocity profile close to the nozzle plane (see top-right figure), which pushes downstream the flame front and ensures the flame stabilizes certain distance from the nozzle plane.

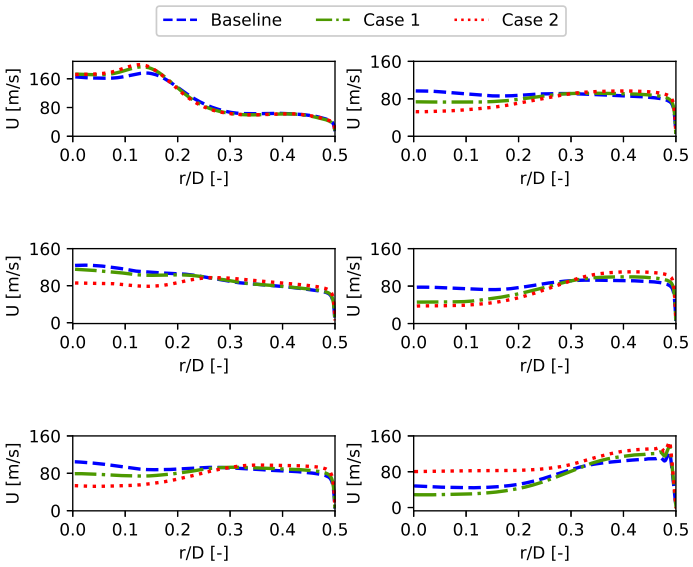

Figure 5 Mean axial velocity at different axial locations across the mixing tube. From left to right and top to bottom: x/M_L=0.09, x/M_L=0.27, x/M_L=0.45, x/M_L=0.63, x/M_L=0.81 and x/M_L=0.90, where x is the axial distance and M_L is the mixing tube length.

Flashback case

The evolution of the flame during a flashback caused by the reduction of axial air injection is shown in Fig. 6 by instantaneous temperature plots at different time instants. The AI is varied using a temporal function that follows a hyperbolic tangent correcting the flow rate of axial air injection and swirl simultaneously to ensure the total mass flow rate is conserved and only the split is changed. The velocity is corrected in 1 ms and the flow is left to evolve until the flashback is produced.

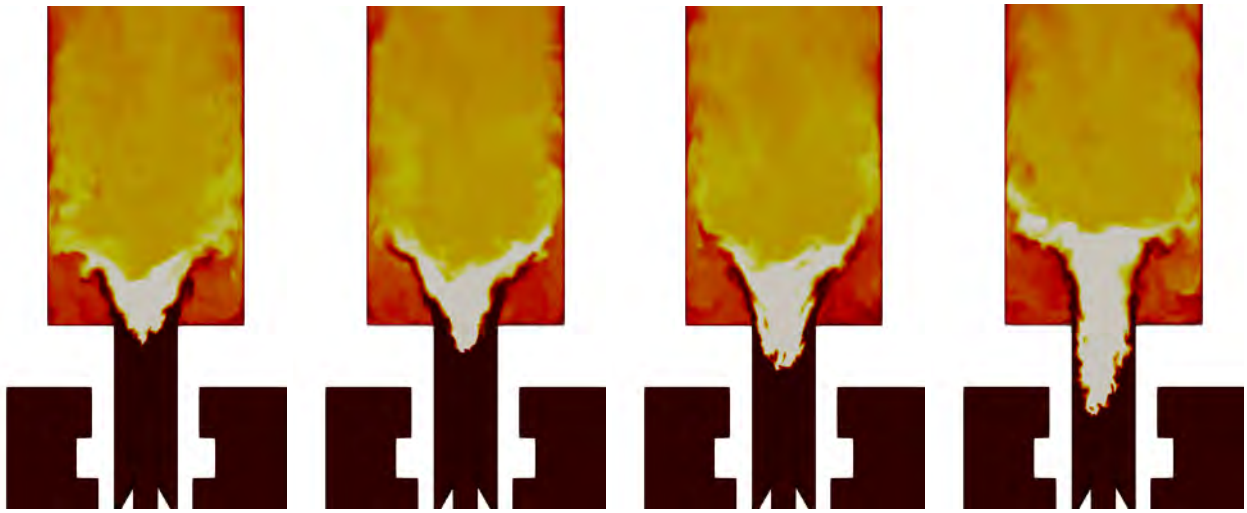

Figure 6 Time evolution of the flame front represented by temperature fields at different time instances during the flashback event. From left to right: time = 1.1 [ms], t = 2.1 [ms], t = 2.5 [ms], and t = 3.05 [ms].

CONCLUSIONS

This work presents a numerical investigation on the stability of a hydrogen flame in a swirl-stabilized burner configuration using large-eddy simulation with tabulated chemistry. The operational conditions simulated in this case are derived

from the stable operation point of the burner for a lean equivalence ratio. From this baseline condition, three computational cases were derived featuring different levels of axial air injection AI respect to the reference case, but keeping the same total mass flow rate and global equivalence ratio. First, a validation of the baseline condition is conducted using PIV from the experimental campaign. Good corrleation for the mean and fluctuating quantities is observed at the location of the flame front. Certain disagreement is found for the RMS at lower axial locations where the coarsening of the mesh is set to reduce the computational cost of the simulation. It is found that as the axial air injection is reduced, the flame tends to stabilize at more upstream locations and the central recirculation zone is also displaced downstream confirming the experimental observations. The penetration of the flame in the mixing tube introduces a strong expansion and acceleration of the flow, which results in a reduction of the spreading angle and eventually a flashback event if the axial air injection is reduced around 25%. An analysis of the burning characteristics of the flame for the different operating conditions is conducted using scatter plots showing a shift towards rich burning as the flame stabilizes towards the mixing tube. Finally, profiles of the velocity field across the mixing tube are presented highlighting the influence of the velocity deficit as a mechanism for flashback resistance.

NOMENCLATURE

AI - Axial Injection
AI_0 - Axial injection baseline
FB - Flashback
Z - Mixture Fraction
T - Temperature
Z_{st} - Stichiometeric mixture fraction
Z_g - Global mixture fraction
U - Velocity [m/s]
U_{RMS} - RMS Velocity [m/s]
r - Radial distance [m]
x - Axial distance [m]
D - Mixing tube diameter [m]
ϕ - Equivalence ratio
Re - Reynolds number
Y_C - Chemical progress variable
C_k - Vreman constant
VB - Vortex breakdown
CRZ - Central re-circulation zone
$\dot{V_{ax}}$ - Axial velocity [m/s]
$\dot{V_{swirl}}$ - Tangential velocity [m/s]
i - Normalized enthalpy
χ - Axial injection rate

ACKNOWLEDGMENTS

The research leading to these results has received funding from the European Union's Horizon 2020 Programme under the CoEC project, grant agreement No. 952181.

REFERENCES

Both, A., Lehmkuhl, O., Mira, D. and Ortega, M. (2020), 'Low-dissipation finite element strategy for low mach number reacting flows', *Computers & Fluids* **200**, 104436.

Burmberger, S. and Sattelmayer, T. (2011), 'Optimization of the aerodynamic flame stabilization for fuel flexible gas turbine premix burners', *Journal of engineering for gas turbines and power* **133**(10).

Che (2016), 'Chemical-kinetic mechanisms for combustion applications'.
URL: *http://combustion.ucsd.edu)*

Cheng, R., Littlejohn, D., Strakey, P. and Sidwell, T. (2009), 'Laboratory investigations of a low-swirl injector with h2 and ch4 at gas turbine conditions', *Proceedings of the Combustion Institute* **32**(2), 3001–3009.

Chterev, I. and Boxx, I. (2021), 'Effect of hydrogen enrichment on the dynamics of a lean technically premixed elevated pressure flame', *Combustion and Flame* **225**, 149–159.

Domingo, P., Vervisch, L. and Veynante, D. (2008), 'Large-eddy simulation of a lifted methane jet flame in a vitiated coflow', *Combustion and Flame* **152**(3), 415–432.

Gövert, S., Mira, D., Kok, J. B., Vázquez, M. and Houzeaux, G. (2018), 'The effect of partial premixing and heat loss on the reacting flow field prediction of a swirl stabilized gas turbine model combustor', *Flow, turbulence and combustion* **100**(2), 503–534.

Khandelwal, B., Karakurt, A., Sekaran, P. R., Sethi, V. and Singh, R. (2013), 'Hydrogen powered aircraft: The future of air transport', *Progress in Aerospace Sciences* **60**, 45–59.

Lee, M. C., Seo, S. B., Chung, J. H., Kim, S. M., Joo, Y. J. and Ahn, D. H. (2010), 'Gas turbine combustion performance test of hydrogen and carbon monoxide synthetic gas', *Fuel* **89**(7), 1485–1491.

Mayer, C., Sangl, J., Sattelmayer, T., Lachaux, T. and Bernero, S. (2012), 'Study on the operational window of a swirl stabilized syngas burner under atmospheric and high pressure conditions', *Journal of Engineering for Gas Turbines and Power* **134**(3).

Mira, D., Jiang, X., Moulinec, C. and Emerson, D. (2014), 'Numerical assessment of subgrid scale models for scalar transport in large-eddy simulations of hydrogen-enriched fuels', *International journal of hydrogen energy* **39**(14), 7173–7189.

Mira, D., Lehmkuhl, O., Both, A., Stathopoulos, P., Tanneberger, T., Reichel, T. G., Paschereit, C. O., Vázquez, M. and Houzeaux, G. (2020), 'Numerical characterization of a premixed hydrogen flame under conditions close to flashback', *Flow, Turbulence and Combustion* **104**(2), 479–507.

Mira, D., Lehmkuhl, O., Stathopoulos, P., Tanneberger, T., Reichel, T., Paschereit, C., Vázquez, M. and Houzeaux, G. (2018), Numerical investigation of a lean premixed swirl-stabilized hydrogen combustor and operational conditions close to flashback, *in* 'Turbo Expo: Power for Land, Sea, and Air', Vol. 51067, American Society of Mechanical Engineers, p. V04BT04A009.

Onarheim, K., Hannula, I. and Solantausta, Y. (2020), 'Hydrogen enhanced biofuels for transport via fast pyrolysis of biomass: A conceptual assessment', *Energy* **199**, 117337.

Palies, P. (2020), *Stabilization and Dynamic of Premixed Swirling Flames*, Academic Press.

Poinsot, T. and Veynante, D. (2005), *Theoretical and numerical combustion*, RT Edwards, Inc.

Reichel, T. G., Goeckeler, K. and Paschereit, O. (2015), 'Investigation of lean premixed swirl-stabilized hydrogen burner with axial air injection using oh-plif imaging', *Journal of Engineering for Gas Turbines and Power* **137**(11).

Reichel, T. G. and Paschereit, C. O. (2017), 'Interaction mechanisms of fuel momentum with flashback limits in lean-premixed combustion of hydrogen', *International Journal of Hydrogen Energy* **42**(7), 4518–4529.

Reichel, T. G., Terhaar, S. and Paschereit, C. O. (2018), 'Flashback resistance and fuel–air mixing in lean premixed hydrogen combustion', *Journal of Propulsion and Power* **34**(3), 690–701.

Reichel, T. G., Terhaar, S. and Paschereit, O. (2015), 'Increasing flashback resistance in lean premixed swirl-stabilized hydrogen combustion by axial air injection', *Journal of Engineering for Gas Turbines and Power* **137**(7).

Sangl, J., Mayer, C. and Sattelmayer, T. (2011), 'Dynamic Adaptation of Aerodynamic Flame Stabilization of a Premix Swirl Burner to Fuel Reactivity Using Fuel Momentum', *Journal of Engineering for Gas Turbines and Power* **133**(7).

Tang, C., Zhang, Y. and Huang, Z. (2014), 'Progress in combustion investigations of hydrogen enriched hydrocarbons', *Renewable and Sustainable Energy Reviews* **30**, 195–216.

Tanneberger, T., Reichel, T. G., Krüger, O., Terhaar, S. and Paschereit, C. O. (2015), Numerical investigation of the flow field and mixing in a swirl-stabilized burner with a non-swirling axial jet, *in* 'Turbo Expo: Power for Land, Sea, and Air', Vol. 56697, American Society of Mechanical Engineers, p. V04BT04A026.

Vázquez, M., Houzeaux, G., Koric, S., Artigues, A., Aguado-Sierra, J., Arís, R., Mira, D., Calmet, H., Cucchietti, F., Owen, H., Taha, A., Burness, E. D., Cela, J. M. and Valero, M. (2016), 'Alya: Multiphysics engineering simulation toward exascale', *Journal of Computational Science* **14**, 15–27.

Vreman, A. (2004), 'An eddy-viscosity subgrid-scale model for turbulent shear flow: Algebraic theory and applications', *Physics of fluids* **16**(10), 3670–3681.

Zheng, Y., Zhu, M., Mira, D. and Jiang, X. (2013), 'Large-eddy simulation of mixing and combustion in a premixed swirling combustor with synthesis gases', *Computers & Fluids* **88**, 702–714.